LASER INDUCED SURFACE EFFECTS

Prepared by

AVCO MISSILES, SPACE AND ELECTRONICS GROUP
SPACE SYSTEMS DIVISION
201 Lowell Street
Wilmington, Massachusetts 01887

AVSSD-0244-67-RR
Contract DA-19-020-AMC-00521 (X)

10 July 1967

Prepared for

BALLISTIC RESEARCH LABORATORIES
UNITED STATES ARMY
ABERDEEN PROVING GROUND
Aberdeen, Maryland

DISCLAIMER NOTICE

THIS DOCUMENT IS BEST QUALITY PRACTICABLE. THE COPY FURNISHED TO DTIC CONTAINED A SIGNIFICANT NUMBER OF PAGES WHICH DO NOT REPRODUCE LEGIBLY.

U.S. ARMY BALLISTIC RESEARCH LABORATORIES
ABERDEEN PROVING GROUND, MARYLAND

ERRATA SHEET 30 AUG 1967

for

AVCO Missiles, Space and Electronics Group Contract Report No. AVSSD-0244-67-RR entitled "Laser Induced Surface Effects" dated 10 July 1967. This Errata Sheet has been compiled by the Contract Monitor, F. J. Allen; it does not include a few (negligible) numerical errors.

1. Page 4, Equation (6) should read:

$$\int \rho \, dx = \frac{1}{\alpha} \ln \frac{I_o}{I} = 2 \int_y^\infty \frac{\rho(r) r \, dr}{\left(r^2 - y^2\right)^{1/2}}$$

2. Page 5, the expression in the middle of paragraph C should read:

$$1.15 \times 10^5 \ cm^2/gm$$

3. Page 12, Equation (15) should read:

$$T = 2T_o/\pi \sin^{-1}\left(\frac{t'}{t}\right)^{1/2} \quad t > t'$$

4. Page 13, Equation (16) should read

$$T = \frac{T_o \delta}{a} + 2T_o \sum_{n=1}^{\infty} \frac{1}{n\pi} \sin \frac{n\pi\delta}{a} \cos \frac{n\pi x}{a} \exp\left(\frac{-n^2\pi^2 Dt}{a^2}\right)$$

Equation (19) should read:

$$T = 2T_o \int_0^{\frac{\delta}{\sqrt{2Dt}}} \frac{1}{\sqrt{2\pi}} \exp\left(-x^2/2\right) dx$$

ERRATA SHEET (contd)

5. Page 14, Equation (21) should read:

$$I_{evap} = 8 \times 10^{13} \exp\left(\frac{-1.03\times10^{5}}{T}\right) \text{ watts/cm}^2$$

line following Equation (21) "Appendix B" should read "Appendix A".

6. Page 17, Equation (29): the z in this equation should be lower case; all z's in the report with the exception of those appearing on page 3 should be lower case.

Equation (30) should read:

$$\int_{-\infty}^{\infty} \rho dx = \frac{2\times5.45\times10^{-4}A}{\sqrt{\pi}}\left(\frac{M}{2RT}\right)^{3/2} z \int_{t'=o}^{t} \frac{e^{-\frac{Mz^2}{2RT(t-t')^2}}\, dt'}{(t-t')^3(t')^{0.575}}$$

7. Page 22, Equation (36) should read:

$$\int_{-\infty}^{\infty} \rho dx = \frac{2}{\sqrt{\pi}}\left(1.02 \times 10^{-2}\right) \pi a^2 \left(\frac{M}{2RT}\right)^{3/2} z \int_{t'=o}^{t} \frac{e^{-\frac{Mz^2}{2RT(t-t')^2}}}{(t-t')^3\left(\frac{t}{\delta}+2.38\times10^{-10} \exp\frac{8.95\times10^{4}}{T_o}\right)^{1.15}} dt'$$

8. Page 23, line 3: $T = 6.1 \times 10^3$ should read $T = 6.3 \times 10^3$.

Paragraph following Equation (38), 4th line: "a factor of 6 too low" should read "a factor of 3 too low".

9. Page 30, Equation (B3) should read:

$$d\rho = \dot{m}\frac{2}{\pi}\left(\frac{M}{2RT}\right)^2\left[v^2 \cos\theta/r^2 \exp\left(\frac{-Mv^2}{2RT}\right)\right] dv$$

ERRATA SHEET (contd)

10. Page 31, Equation (B8) should read:

$$d \int_{-\infty}^{\infty} \rho dx = \frac{8}{\sqrt{\pi}} \dot{m}\, z \left(\frac{M}{2RT}\right)^{3/2} (t - t')^{-3} \exp\left[-\frac{Mz^2}{2RT(t-t')^2}\right]$$

$$\left(\int_{0}^{a} \sqrt{a^2 - y^2} \exp\left[-\frac{My^2}{2RT(t-t')^2}\right] dy\right) dt'$$

In this equation y is to be regarded as a variable of integration; it refers to a coordinate in the source plane and is not the same as the y above.

11. Page 32, Equation (B13) should read:

$$d \int_{-\infty}^{\infty} \rho dx = 2\sqrt{\pi}\, a^2 \dot{m}\, z \left(\frac{M}{2RT}\right)^{3/2} (t - t')^{-3} \exp\left[-\frac{Mz^2}{2RT(t-t')^2}\right] dt'$$

12. Page 34, Equation (B15) should read:

$$1.5(t - t')^2 = \frac{Mz^2}{2RT}$$

13. Page 35, Equation (B20) should read:

$$\int_{-\infty}^{\infty} \rho dx = 1.64\, \dot{m}\, a \left(\frac{M}{2RT}\right)^{1/2} \left[\exp\left(-\frac{Mz^2}{2RTt^2}\right) - \exp\left(-\frac{Mz^2}{2RT\{t-t'\}^2}\right)\right]$$

Equation (B21) should read:

$$\int_{-\infty}^{\infty} \rho dx = \frac{1.77\, \dot{m}\, a^2}{z} \left(\frac{M}{2RT}\right)^{1/2} \left[\exp\left(-\frac{Mz^2}{2RTt^2}\right) - \exp\left(-\frac{Mz^2}{2RT\{t-t'\}^2}\right)\right]$$

This document consists of 40 pages,
126 copies, Series A

LASER INDUCED SURFACE EFFECTS

Prepared by

AVCO MISSILES, SPACE AND ELECTRONICS GROUP
SPACE SYSTEMS DIVISION
201 Lowell Street
Wilmington, Massachusetts 01887

AVSSD-0244-67-RR
Contract DA-19-020-AMC-00521 (X)

10 July 1967

Prepared for

BALLISTIC RESEARCH LABORATORIES
UNITED STATES ARMY
ABERDEEN PROVING GROUND
Aberdeen, Maryland

ABSTRACT

This document presents the results of experiments in which a moderate energy electron beam was used to probe the plasma created by a laser beam impinging on a graphite target.

EDITED BY:
EDITORIAL SERVICES SECTION
A. C. J. Petralia

CONTENTS

ILLUSTRATIONS

SUMMARY

This report contains the results of experimental work performed under Contract DA-19-020-AMI-00521(X), "Laser Induced Surface Effects." A moderate energy electron beam was used to probe the plasma created by a laser beam impinging on a graphite target. The attenuation of the beam was used to determine the amount of material traversed by the beam. Although the original expectation was that this technique would be extremely useful in probing the vapor near the target at times which were comparable to the overall laser pulse duration, the results indicate that the bulk of the observed results were due to vapor thermally emitted from the target at times which were long compared to the laser pulse. This effect has been observed for graphite. However, no experiments have been performed which could confirm this effect for other materials. The experimental work on the electron beam technique was initially performed by Dr. H. Furumotu. The experimental results reported herein were obtained by L. Pettingill and J. Shumsky. The interpretation of the results and preparation of the report was performed by R. Schlier.

I. INTRODUCTION

During the past several years, a number of different techniques have been used at Avco to investigate the physical phenomena which occur during and after the interaction of intense laser radiation with solid targets. All of these techniques have been intended to probe the properties of the vapor created by the interaction, since the vapor dominates the interaction at high intensity levels.

The experiments that have been performed include: (1) measurement of impulse transferred to the target; (2) measurement of velocity distribution of the plasma created by the interaction, at times long when compared to the laser pulse; (3) measurement of electron density in the plasma during and after the laser pulse; and (4) measurement of electron temperature in the plasma. In the present report, a fifth measurement technique is described -- this consists of measurement of mass density of the vapor at distances close to the target.

Before describing the actual experiment, it would be well to state the understanding of the phenomena as it existed at the time the experiment was undertaken. Let us consider a solid target which is irradiated by a short-duration, intense laser beam. If the target is metallic, the laser radiation is reflected and absorbed. Since the metallic target has a large extinction coefficient for optical radiation, it is reasonable to assume that the absorption of the radiation occurs at the geometrical surface, rather than in the volume near the surface; consequently, the surface is rapidly heated until appreciable evaporation can occur. However, the temperatures that can be attained by the surface are sufficiently high that a large amount of thermionic electrons and metallic ions are emitted from the hot surface. These ions and electrons form the basis for further absorption of laser energy by the vapor. In particular, the electrons present can gain sufficient energy from direct excitation by the intense radiation, causing further ionization to occur. The vapor then becomes highly ionized and very absorbing to the radiation. Thus, the larger part of the laser energy is deposited in the vapor, rather than the solid, and the vapor attains a very high temperature and a very high expansion velocity.

This qualitative description has been based on the experimental observations mentioned above. The expansion velocities observed are on the order of 3×10^6 cm/sec, corresponding to particle energies of several hundred electron volts. The observed vapor temperatures are as high as 40 electron volts. The electron density measurements indicate that the vapor is very nearly fully ionized. The high velocities, in particular, are too large to be accounted for by any reasonable surface temperature and are, in themselves, adequate evidence of vapor absorption. Vapor absorption has also been confirmed by direct measurement of the optical opacity of the vapor.

The mass density experiment was intended to provide additional information on the details of the interaction process. From the qualitative description above, one would expect that the mass density close to the surface would show a maximum shortly after the onset of the laser pulse, and decrease rapidly as the rate of evaporation decreased. The decrease in the rate of evaporation would be expected if the direct laser radiation was prevented from reaching the surface by the opaque vapor. A mass density measurement would also be expected to show the presence of shock phenomena in the vapor.

II. EXPERIMENTAL PROCEDURE

A. CONCEPT

The basic concept of the mass density measurement is to direct a beam of high-energy electrons (20-30 kev) through the plasma in front of the target, and to measure the attenuation of the beam as a function of time. At these high electron energies, the atoms or molecules in the path of the electron beam act as Rutherford scatterers, with the bulk of the scattering being caused by the electrostatic field of the nucleus. Thus, the state of the scattering medium is not of great significance, and the amount of scattering depends primarily on the number of atoms in the path of the beam.

Rutherford scattering is highly angular-dependant. The differential scattering cross section for an atom of atomic number Z, for electrons of energy E, can be written as

$$\sigma(\theta) = \frac{e^4 Z^2}{16 E^2 \sin^4(\theta/2)} \tag{1}$$

On insertion of numerical values and electron energies in kev, this equation becomes

$$\sigma(\theta) = 1.29 \times 10^{-21} Z^2/E^2 \sin^4(\theta/2) \text{ cm}^2 \tag{2}$$

The total cross section, determined by integrating the differential cross section, is infinite. In actual practice, however, one will collect all electrons which are scattered by less than some angle θ_o, so that the attenuation cross section is

$$\sigma = 1.29 \times 10^{-21} (Z/E)^2 \, 2\pi \int_{\theta_o}^{\pi} \sin\theta \, \sin^{-4}(\theta/2) \, d\theta$$

$$\sigma = 1.29 \times 10^{-21} (Z/E)^2 \, 4\pi \cot^2(\theta_o/2) \text{ cm}^2 \tag{3}$$

In a carefully designed experiment, θ_o can be made as small as 10^{-2} radians, so that

$$\sigma = 6.5 \times 10^{-16} (Z/E)^2 \text{ cm}^2 \tag{4}$$

For graphite, $Z = 6$, and a typical electron beam energy is 25 kev. Thus, the attenuation cross section per particle could be as large as 3.75×10^{-17} cm^2.

From previous work, we can make a very rough estimate of the mass density near the target. It has been observed that, for an incident energy of about 1 joule on 10^{-2} cm^2 area, about 10^{-6} grams of material are removed. This material has a velocity in the vicinity of 3×10^6 cm/sec, for graphite. If we assume that the material leaves the target over a time approximately that of the laser pulse duration (5×10^{-8} seconds), we would expect a mass density near the target region of about 6.7×10^{-4} gm/cm^3.

If we propagated an electron beam along a line parallel to the target, through the center of the area, the beam would travel a distance of 1.1×10^{-1} cm, so the beam would encounter an integrated density of about 7.4×10^{-5} gm/cm^2, or 3.7×10^{18} particles for graphite. With the attenuation cross section given above, the beam would be attenuated by a factor of e^{139}, so that it is obvious that a much lower coefficient is needed. However, lowering of the coefficient can be accomplished by increasing the effective aperture of the detector of the electron beam. By increasing θ_o to 5×10^{-2} radians, the attenuation cross section is decreased by a factor of 25, and the attenuation is now a factor of $e^{5.56}$ or 260. This is still large, but it is in the vicinity of experimental feasibility. Other effects, such as shielding of the nucleus by outer electrons, would be expected to decrease the attenuation cross section to some extent. Our estimate of mass density may also be somewhat high.

The experimental observations, then, consist of determining the transmitted electron beam current as a function of time. The time is to be related to the time of onset of the laser pulse. The integrated density encountered by the beam can then be determined from the equation

$$I = I_o \exp - a \int \rho \, dx \tag{5}$$

where I is the instantaneous beam current, I_o the current in the absence of attenuation, a a calibration constant to be determined either experimentally or from the equations for Rutherford scattering, and ρ the mass density.

If the electron beam is propagated along a line parallel to the target surface, at a fixed distance z from the target, and several observations are made at different locations of the beam from the central axis of the laser beam, it is possible to determine the mass density, for a given time, as a function of z and the radius from the central axis, provided the blowoff pattern is symmetrical about this axis. The mass density is assumed to be a function of z, r, and t. The observed integrated density is a function of z, y, and t. The integrated density is related to the mass density by the equation

$$\int \rho \, dx = \frac{1}{a} \ln \frac{I_o}{I} = 2 \int_y^\infty \frac{r \, dr}{\sqrt{r^2 - y^2}} \tag{6}$$

This equation is one form of the Abel equation, and its inverse is

$$\rho(r, z, t) = -\frac{1}{\pi} \int_{r}^{\infty} \frac{\frac{d}{dy}\left(\int \rho \, dx\right)}{\sqrt{y^2 - r^2}} \, dy \tag{7}$$

A number of numerical methods exist for the determination of ρ from values of $\int \rho \, dx$ determined at several different distances y from the axis.

B. APPARATUS

Successful completion of the mass density experiment presented some serious problems earlier. In particular, the copious amount of ultraviolet radiation emitted by the plasma in front of the target caused some serious effects. This radiation caused a great deal of photoelectric emission from the electron-beam detector electrode, which in the initial experiments, was a Faraday box. This emission caused a spurious signal.

The detector problem was eliminated by replacing the detector with a scintillating material. A thin metallic film on the surface prevented direct electromagnetic radiation from reaching the scintillator. A photomultiplier was used to view the light emitted when electrons passed through the film into the scintillator.

A second problem was then discovered: the ultraviolet radiation also struck the electrodes of the electron gun which produced the beam. Since these electrodes were at a high negative potential, the resultant photoelectric emission caused an appreciable defocusing of the beam, and again, a spurious signal was observed. In order to eliminate this problem, as part of the current work, the apparatus shown schematically in Figure 1 was designed. Here there is no direct optical path from the target to the electron gun; the beam passes through optical baffles and is magnetically deflected to pass near the target.

C. CALIBRATION OF THE ELECTRON BEAM

The attenuation coefficient α was determined by passing the electron beam through a thin graphite film. This coefficient was determined to be about

$$1.15 \times 10^{-5} \ cm^2/gm$$

This corresponds to an attenuation cross section of 2.3×10^{-18} cm^2, which is the cross section to be expected if $\theta_o = 0.04$ radian.

D. EXPERIMENTAL PROCEDURE

Figure 2 shows a schematic of the experimental arrangement. To turn on the electron beam prior to the actual laser pulse, a trigger pulse was derived from the fluorescent radiation reflected off the rotating mirror of the laser oscillator. The position of the pickup of this radiation could be adjusted to provide a trigger about 50 microseconds before the laser pulse.

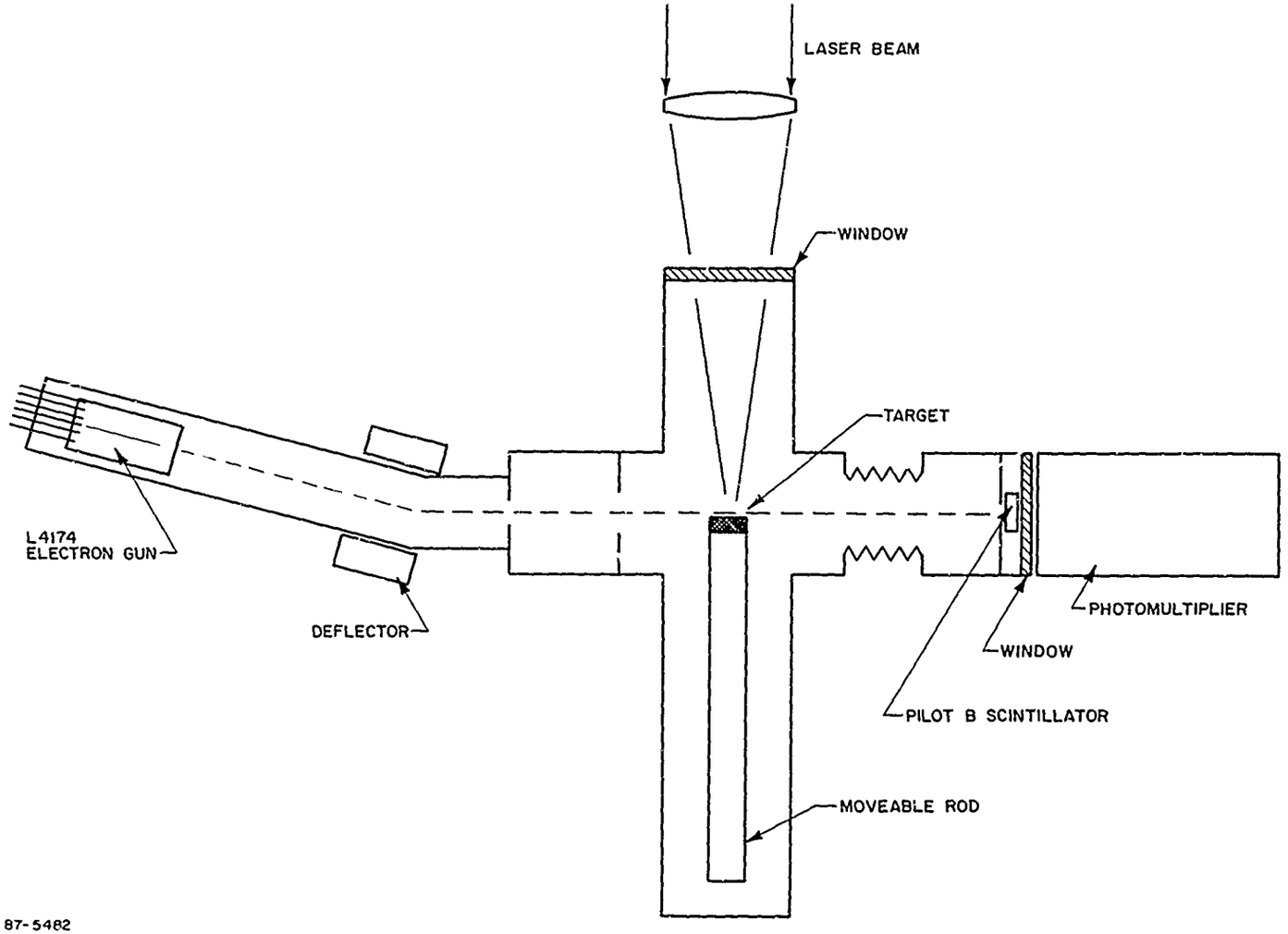

Figure 1 ELECTRON BEAM APPARATUS

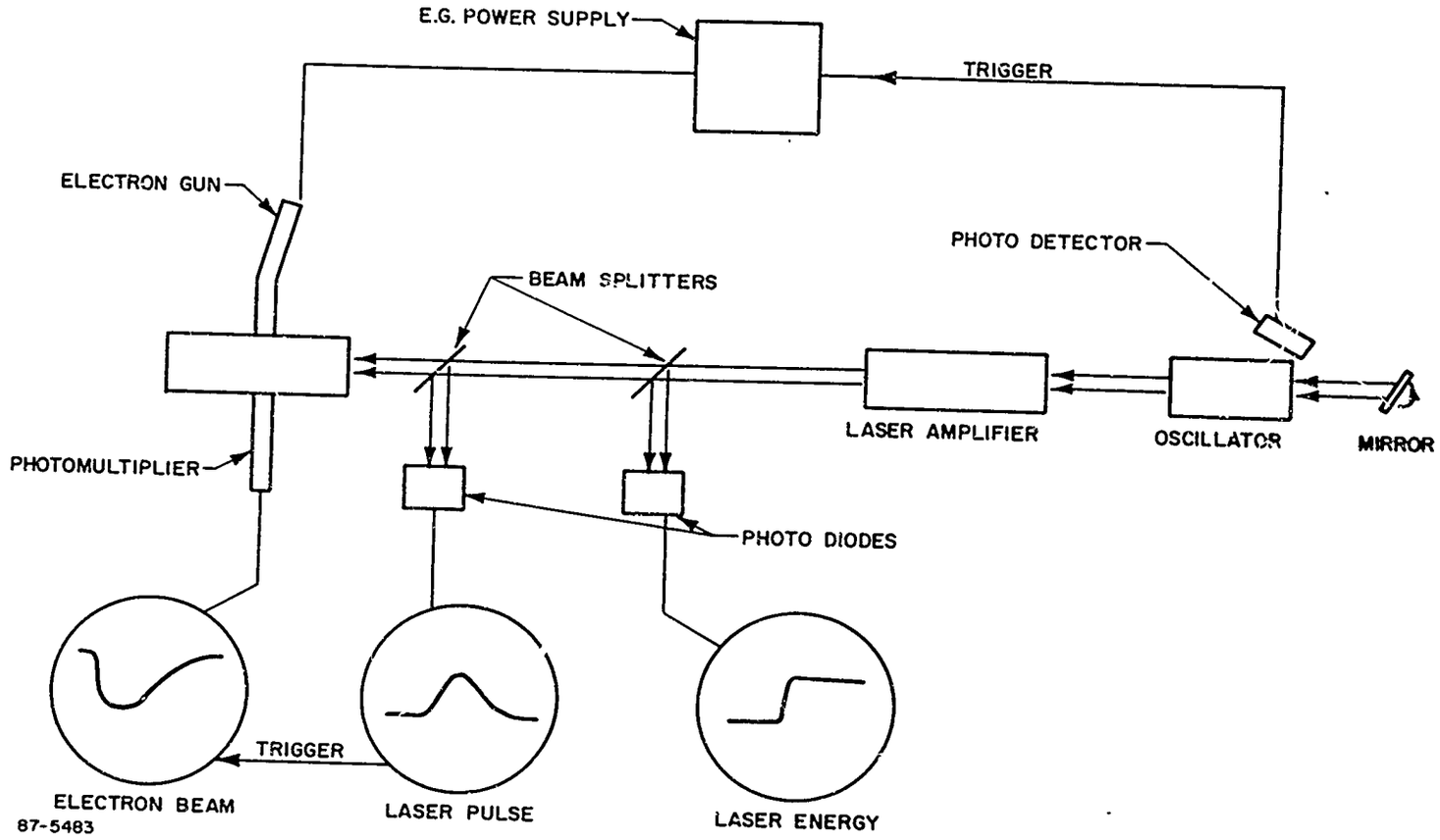

Figure 2 ARRANGEMENT

The laser peak power and pulse shape was determined with the aid of a beam splitter outside the experimental chamber, a planar diode, and a Tektronix 519 oscilloscope. The oscilloscope was triggered internally with the laser pulse signal. The trigger pulse from the oscilloscope was also used to trigger a second oscilloscope which recorded the actual electron beam current. A second beam splitter and photodiode were used to provide a time-integrated measurement of the laser output. Both photodiodes were calibrated against a water-filled calorimeter placed in the target position inside the apparatus.

The electron beam was kept in essentially the same position during all of the firings. The position of the laser-beam axis with respect to the electron beam was adjusted by a vertical translation of the lens used to focus the beam on the target. The distance between target and beam was adjusted by a translation of the target, and the laser beam size, at the target, was controlled by adjusting the focusing lens. The target was mounted on a rod which could be rotated. When the laser beam was deliberately focused off the axis of rotation, it became possible to rotate the target between firings, presenting a fresh surface to the laser beam, thus preventing excessive hole-drilling effects.

III. INTERPRETATION OF RESULTS

A. EXPERIMENTAL RESULTS

A typical experimental result is shown in Figure 3, where the integrated density (the mass density projected along the line of the electron beam) in gm/cm^2 is plotted as a function of time after initiation of the laser pulse.

All of the experimental data has the same qualitative appearance -- a peak integrated density at about 0.5 microsecond after the laser pulse, and observable effects for about 2 microseconds. This is in direct contrast to the results expected, if the velocity distributions observed with the microwave cavity technique dominated the density close to the target. At the intensity used, the average velocity of the plasma as observed with the cavity technique is on the order of 10^7 cm/sec. Thus the peak integrated density should occur during the laser pulse (in less than 3×10^{-8} seconds).

We are therefore faced with the serious problem of accounting for the observed electron beam results. At the same time, it must be kept in mind that the observations with the microwave cavity indicate much higher velocities than can be inferred from the electron beam results.

The microwave cavity data indicate that the average velocity of the plasma at the intensity used for Figure 3 is about 5×10^6 cm/sec, and that the average kinetic energy is about 4×10^{-10} erg/atm. The total mass of vapor contributing to the observed cavity data can be estimated by assuming that about 50 percent of the laser energy went into kinetic energy of the vapor. For graphite, this results in a mass loss of about 0.25×10^{-6} gm/joule (for the example given in the figure, about 3.3×10^{-7} gm). This vapor is emitted during the laser pulse (about 50 nanoseconds), so that the mass evolution rate is about 6.5 gm/sec.

For the sake of calculation, let us assume that during the laser pulse the vapor can be characterized by a velocity distribution typical of evaporation from a surface at a temperature T. From kinetic theory, this distribution can be written as

$$F(v)\,dv\,d\Omega = \frac{2}{\pi}\,(M/2RT)^2\,v^3\,\cos\theta\,(\exp - Mv^2/2RT)\,dv\,d\Omega \qquad (8)$$

where $F(v)\,dv\,d\Omega$ is the fraction emitted in the velocity range v to $v + dv$, in the direction θ, and the solid angle $d\Omega$. M is the molecular weight, R the gas constant, and T the absolute temperature. From this distribution, the average kinetic energy is

$$E = 2\,RT\ erg/molc \qquad (9)$$

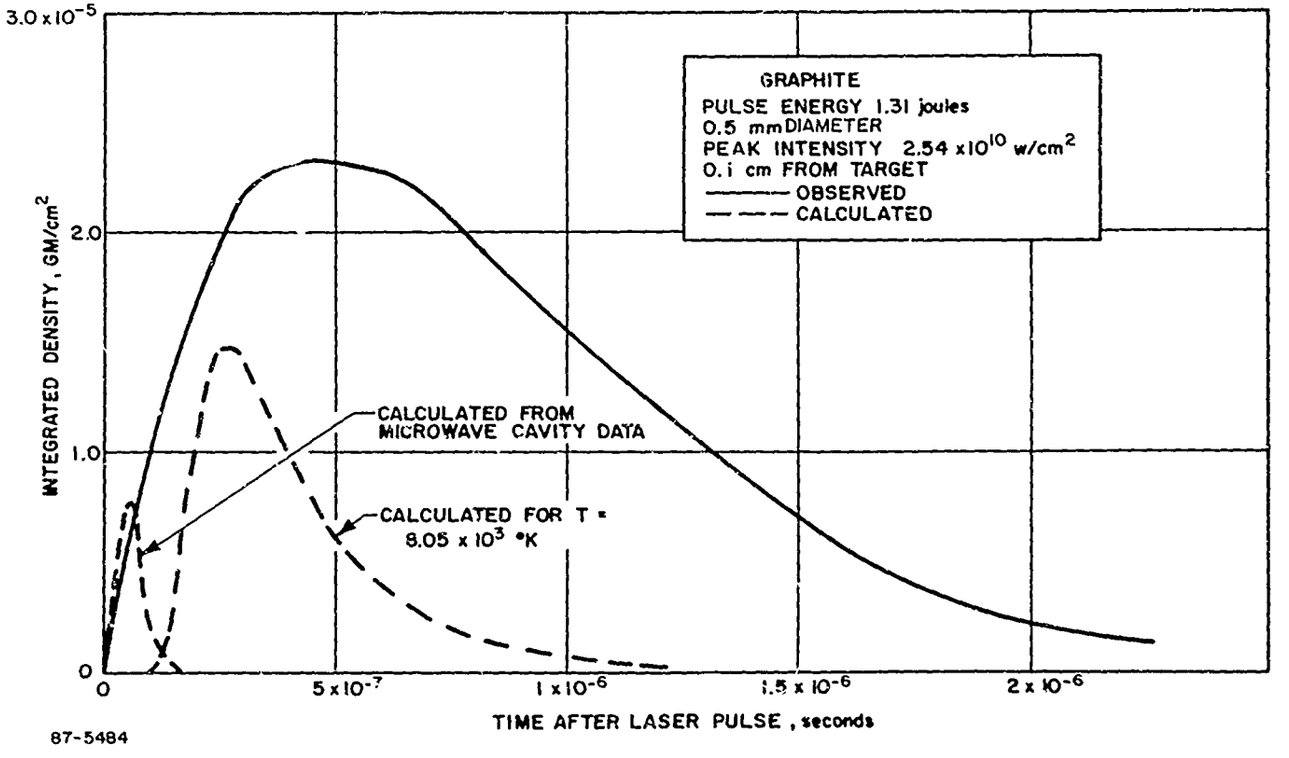

Figure 3 INTEGRATED DENSITY OBSERVATIONS

and the average velocity is

$$\bar{v} = \frac{3\,(2\pi RT/M)^{1/2}}{4} \quad cm/sec \tag{10}$$

Fitting the kinetic energy with the observed energy, we get a temperature of 1.45×10^6°K, and from the velocity we get $T = 10^6$°K.

Appendix B shows that for the case given, the integrated density can be expressed by the equation

$$\int_{-\infty}^{\infty} \rho\, dx = 1.77\, \dot{m}\, a^2\, (M/2RT)^{1/2}\, z^{-1} \{ exp\,(-Mz^2/2RT\,t^2) - exp\,[-Mz^2/2RT\,(t-t')^2] \} \tag{11}$$

where $\dot{m}$ is the mass evaporation rate per unit area, a the irradiated radius, z the distance of the beam from the surface, t' the laser pulse duration, and t is the time after the start of the laser pulse. In plotting the expression, the second term on the right-hand side is zero for $t \leq t'$. We can evaluate this expression for $z = 0.1$ cm, $\pi \dot{m} a^2 = 6.5$ gm/sec, $T = 10^6$°K, $M = 12$ and $R = 8.31 \times 10^7$ erg/mole-°K.

$$\int_{-\infty}^{\infty} \rho\, dx = 9.85 \times 10^{-6} \{ exp\,(-7.22 \times 10^{-16}/t^2) - exp\,[-7.22 \times 10^{-16}/(t-5 \times 10^{-8})^2] \} \tag{12}$$

This expression is also plotted in Figure 3. As can be seen, the contribution for the high-velocity species is significant only at short times, and we must seek another means of accounting for the data.

This discrepancy between the microwave cavity data and the electron beam data is only apparent at the short distances of the electron beam experiment. At long distances, the electron beam experiment is not applicable (densities would be too low for detection), and the microwave cavity is only sensitive to the electrons present in the high-velocity plasma.

In order to account for the observations, it appears necessary to postulate at least two components of the vapor emitted. One component is the fast vapor which results from the absorption of laser energy by the vapor near the target. This component is significant only at "short" times, and does not contribute to the bulk of the observed density. The second component can be assumed to be thermally emitted by the hot target surface, both during and after the laser pulse. Most of the vapor emitted during the laser pulse, however, is further heated, and is therefore not a major contributor to the "slow" component. Let us assume, however, that perhaps an amount of vapor equal to the fast component is also emitted during the pulse, but is not accelerated, and therefore has a

temperature characteristic of the surface. This temperature can be estimated from the mass loss rate, by means of the approximate equation

$$\dot{m} = 1.2 \times 10^{9} \exp(-1.03 \times 10^{5}/T) \tag{13}$$

The expression is an approximation to the published data on the rate of graphite evaporation as a function of temperature, and is more fully derived in Appendix A. In the case of Figure 3,

$$\dot{m} = \frac{6.5}{\pi a^{2}}$$

and πa^{2} is 2×10^{-3} cm^{2}. Hence $T = 8.05 \times 10^{3}$.

Applying this temperature to the equation for integrated density, we have

$$\int_{-\infty}^{\infty} \rho \, dx = 1.0 \times 10^{-4} \left| \exp(-9.00 \times 10^{-14}/t^{2}) - \exp[-9.00 \times 10^{-14}/(t-5 \times 10^{-8})^{2}] \right| \tag{14}$$

This expression is also plotted on Figure 3. With allowance for a longer low-velocity tail on the high-velocity component, it appears that the combined effects of the two components, emitted during the laser pulse, can account for the early part of the observed integrated density function. However, the temperature which one must assume in order to fit Equation (11) to the observed integrated density at longer times is only about 10^{3}°K. At this temperature, the rate of evaporation is negligible, being over 30 orders of magnitude too low. We therefore must conclude that the observations can not be reconciled with the assumption that all of the evaporation occurs at times which are of the same duration, or perhaps longer by a factor of 2, as the laser pulse. We must postulate that appreciable evaporation occurs after the pulse.

B. SURFACE COOLING

First, it is important to determine whether or not such evaporation is realistic. During the laser pulse, the temperature at the surface is nearly constant, since most of the energy incident on the surface from the laser beam is used to evaporate material from the surface. If all of the incident energy is absorbed at the surface, and if the thermal conductivity of the graphite is constant, then the surface temperature can be shown to be approximately

$$T = T_{o} \qquad t < t'$$

$$T = (2T_{o}/\pi) \sin^{-1} t'/t \qquad t > t' \tag{15}$$

The decay of temperature is much too fast to allow appreciable evaporation from the surface, at times longer than the laser pulse. There are, however, two mechanisms which may allow a much slower decay time. In the first place, the thermal conductivity of the graphite would be expected to be much higher at elevated temperatures than at room temperature. In the second place, there is a great deal of thermal reradiation from the vapor during the laser pulse. Since this radiation occurs at short wave lengths, it is not unreasonable to expect that it penetrates relatively deeply into the surface, and that consequently, the surface layer is heated to a relatively high temperature for an appreciable depth. In the absence of losses, the surface layer will remain hot for an appreciable time, since thermal conductivity into the interior is relatively low for graphite. We can estimate the time required for an appreciable change in surface temperature by assuming that the temperature of the graphite was T_o at the end of the laser pulse, for a distance δ into the surface. If only thermal conduction is considered, the temperature of the graphite can be expressed by the equation

$$T = \frac{T_o \delta}{z} + 2T_o \sum_{n=1}^{\infty} \frac{\sin \frac{n\pi\delta}{a}}{n\pi} \cos \frac{n\pi x}{a} \exp \frac{-n^2 \pi^2 D t}{a^2} \tag{16}$$

where D is the thermal diffusivity of the graphite, and a is the thickness of the graphite. If a is large, the temperature at the surface is

$$T = (2T_c/\pi) \int_0^{\infty} u^{-1} (\sin u\delta) (\exp - u^2 Dt)\, du \tag{17}$$

where the summation has been replaced by an integration. The integral can be shown to be equivalent to the integral

$$T = T_o (\pi Dt)^{-1/2} \int_0^{\delta} \exp - u^2/4Dt \; du \tag{18}$$

This integral can be rewritten in the form of the probability integral

$$T = 2T_o \int_0^{\delta/\sqrt{2Dt}} \frac{1}{2\pi} (\exp - x^2/2)\, dx \tag{19}$$

which is a tabulated function. Figure 4 is a plot of T/T_o as a function of $2Dt/\delta^2$. It can be seen that the decrease in temperature is negligible for $2Dt/\delta^2$ less than 0.1. Since D for graphite is about 0.01, the time required for detectable cooling is $t = 5.0\ \delta^2$, for δ in cm. To decrease the temperature by 10 percent requires $20\ \delta^2$ seconds.

Thus, if the heated layer were only 3 microns thick, approximately 2×10^{-6} seconds would be required to cool the surface by 10 percent, by conduction alone. The surface temperature is not expected to reach more than 10,000°K. A 3-micron layer would thus store approximately 6 joule/cm^2 of energy. Since, under the conditions of the experiment, total energy deliveries to the surface are on the order of 100 to 1000 joule/cm^2, it appears that sufficient energy is available, even if only a fraction penetrates to cause heating of a sufficiently thick layer.

It is apparent, then, that if a sufficiently thick surface layer is heated, the losses by evaporization and radiation from the surface must dominate the cooling process. The loss by radiation cannot exceed the blackbody limit

$$I_{rad} = 5.67 \times 10^{-12}\ T^4\ watt/cm^2. \tag{20}$$

The loss due to evaporation can be approximated by the expression

$$I_{evap} = 8 \times 10^{-13}\ exp\,(-1.03 \times 10^5/T)\ watt/cm^2 \tag{21}$$

Equation (21) is also derived in Appendix B.

Evaporation losses will exceed radiative losses for all temperatures above 4200°K, and therefore radiation can be neglected.

For times during which the effect of thermal conduction into the interior can be neglected, the cooling rate of the surface can be approximated by the cooling rate that the surface of an infinitely thick slab, initially at a temperature T_o, would undergo.

Suppose we have a very thick material which is heated with an input flux I at the surface. Then the temperature at a time t, after heating for an incremental time $\Delta t'$, is

$$T = I\ \Delta t'/(\pi\ \rho\ CK\ t)^{1/2} \tag{22}$$

If I is a function of t', then, at a time t later than t', we have

$$dT/dt' = \frac{I}{[\pi\ \rho\ CK\ (t - t')]^{1/2}} \tag{23}$$

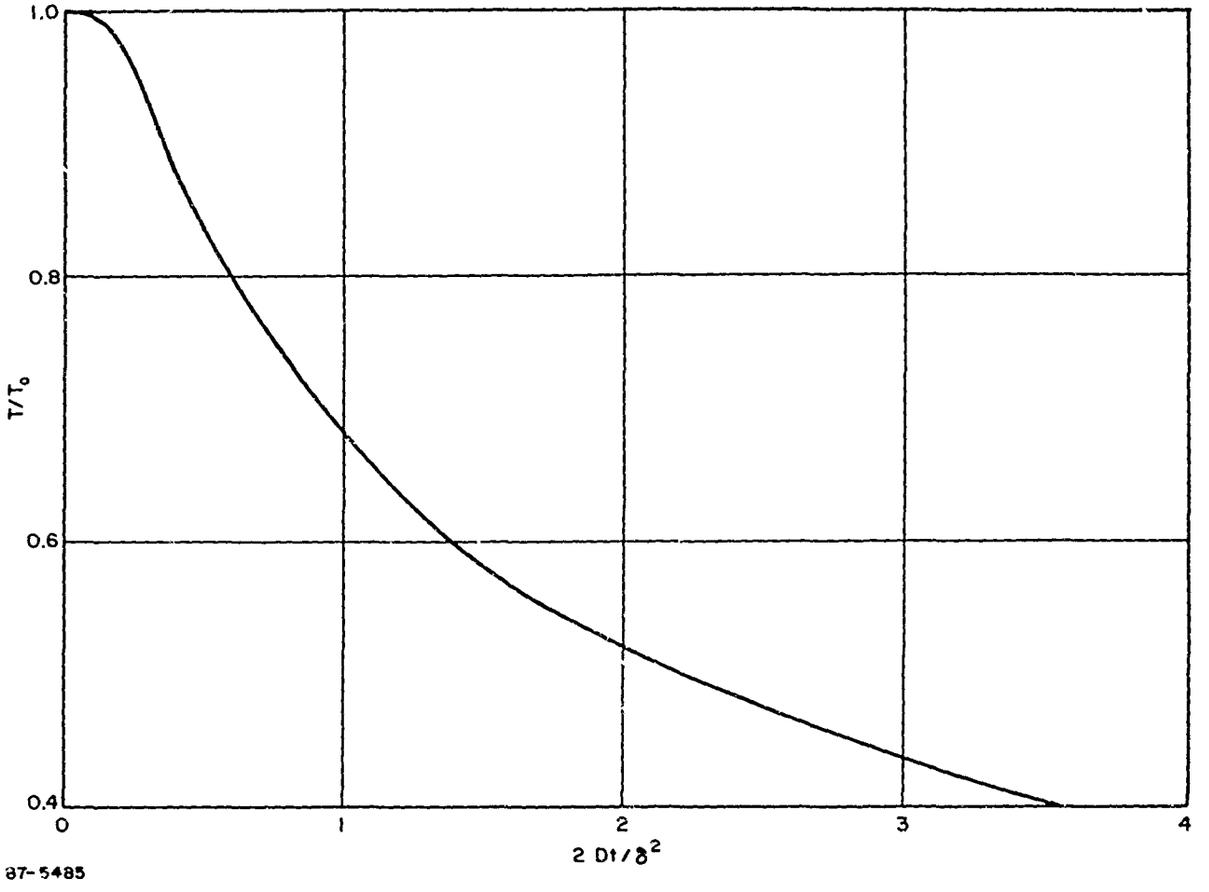

Figure 4 COOLING OF GRAPHITE BY CONDUCTION

Since heat equation solutions can be superposed, the temperature at the surface is then the integral of this expression over the time of the heat flux I. Alternatively, if I is a function of temperature, we have

$$-[I(T)]^{-1}\,dT = (\pi\rho CK)^{-1/2}(t-t')^{-1/2}\,dt' \tag{24}$$

which is to be integrated from $t' = 0$ to $t' = t$. Thus

$$-\int_{T_o}^{T} I(T)^{-1}\,dT = 2\,t^{1/2}/(\pi\rho CK)^{1/2} \tag{25}$$

For our case, $I(T) = 8 \times 10^{13} \exp(-1.03 \times 10^5/T)$ and we have

$$-\int_{T_o}^{T} (\exp 1.03 \times 10^5/T)dT = 16 \times 10^{13}\,t^{1/2}/(\pi\rho CK)^{1/2} \tag{26}$$

Equation (26) is not analytically integrable. However, a numerical integration followed by a curve-fit results in a fairly good approximation to the integral

$$3.81 \times 10^3 (\exp\ 8.95 \times 10^4/T - \exp 8.95 \times 10^4/T_o) \tag{27}$$

$$= 1.6 \times 10^{14}\,t^{1/2}/(\pi\rho CK)^{1/2}$$

If we now use the equation for $\dot{m}$ as a function of T, we obtain an expression for the mass evolution rate as a function of time:

$$\dot{m} = 5.45 \times 10^{-4}\,(t^{1/2} + 1.89 \times 10^{-11} \exp 8.95 \times 10^4/T_o)^{-1.15} \tag{28}$$

Over most of the range in t, the evolution is reasonably well represented by the simpler expression

$$\dot{m} = 5.45 \times 10^{-4}\,t^{-0.575}\ gm/cm^2 - sec \tag{28a}$$

Equation (27) can also be used to provide an approximate expression for the temperature.

$$T = 8.95 \times 10^4 \, (\ln 5.29 \times 10^{10} \, t^{1/2})^{-1} \tag{27a}$$

Equation (27a) is plotted in Figure 5. As can be seen, the temperature is very nearly constant over a wide range in time.

C. ESTIMATED DENSITY

We have shown that it is not unreasonable to expect that the temperature of the graphite surface will remain high for a relatively long time following the laser pulse. To be sure, the temperature drops rapidly at first, but it remains in the vicinity of 5000°K for an appreciable time.

We will use the same form used to derive the density for a constant temperature evolution. The integrated density, due to evaporation during a short increment of time dt', can be expressed as

$$d \int_{-\infty}^{\infty} \rho \, dx = \frac{2 \dot{m} A}{\sqrt{\pi}} \left(\frac{M}{2RT} \right)^{3/2} \frac{Z \, e^{-\frac{M z^2}{2RT (t - t')^2}}}{(t - t')^3} \, dt' \tag{29}$$

Although both $\dot{m}$ and T in this expression are functions of time, the value of T varies very slowly in time. Thus we are justified in replacing T by an average. The average value of T can be estimated by using the value of T that would give the same total mass emission in a time of about 1 microsecond. The total mass emission in 10^{-6} seconds, according to the approximate expression for mass evaporation rate, is 3.6×10^{-6} gm/cm^2. This would correspond to a constant temperature of 5.25×10^3°K. The integrated density, at a time t, then becomes

$$\int_{-\infty}^{\infty} \rho \, dx = \frac{2 \times 5.45 \times 10^{-4} A}{\sqrt{\pi}} \left(\frac{M}{2RT} \right)^{3/2} z \int_{t'=0}^{t} \frac{e^{-\frac{M z^2}{2RT (t - t')}}}{(t - t')^3 \, (t')^{0.575}} \, dt' \tag{30}$$

If we let $u^2 = 2RT \, t^2 / M z^2$, we have

$$\int_{-\infty}^{\infty} \rho \, dx = \frac{(2)(5.45 \times 10^{-4}) A}{\sqrt{\pi}} \left(\frac{M}{2RT} \right)^{0.2125} z^{-1.575} \int_0^u \frac{e^{-\frac{1}{(u - u')^2}}}{(u')^{0.575} (u - u')^3} \, du' \tag{31}$$

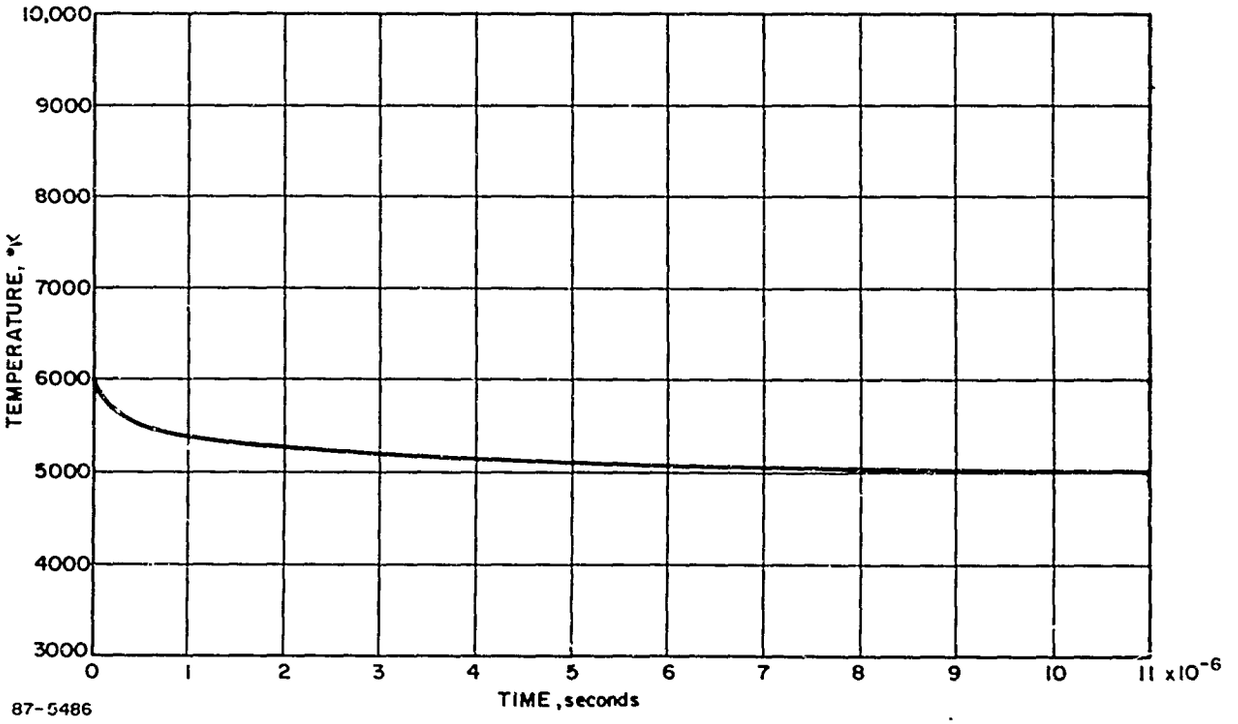

Figure 5 COOLING OF GRAPHITE BY EVAPORATION

For $M = 12$, $T = 5.25 \times 10^3$, $z = 0.1$ we have

$$\int_{-\infty}^{\infty} \rho \, dx = 1.13 \times 10^{-4} \int_0^u \frac{e^{-\frac{1}{(u-u')^2}}}{u'^{0.575}\,(u-u')^3} \, du' \qquad (-?)$$

where

$$u = 2.7 \times 10^6 \, t$$

The integral again is not analytic, but can be numerically evaluated. The integral is given in Figure 6.

The maximum value of the integral is 0.68, occurring at $u = 1.2$. For the case in Figure 3, $A = 2 \times 10^{-3}$ cm^2, giving a maximum integrated density of $1.5^4 \times 10^{-7}$ gm/cm^2 at a time of 4.4×10^{-7} seconds. The time is in good agreement with observation, but the value of the maximum is about two orders of magnitude too low. However, it should be recalled that the room temperature value of graphite thermal conductivity was used to calculate the mass loss rate. If the thermal conductivity were to be increased by a factor F, the equation for mass loss rate would be increased by the factor $F^{0.575}$. Furthermore, it is not at all unreasonable to postulate that the area heated by re-radiation from the vapor would be larger than the focal area of the beam. An area increase by a factor of 10 does not appear to be too much for a focal diameter of only 0.05 cm. The high-velocity plasma travels a distance of about 0.25 cm during the laser pulse so that irradiation of a comparable diameter at a high intensity level might be expected to occur. An increase in thermal conductivity by a large factor might also be realistic. It is therefore not unreasonable to normalize the calculated integrated density to fit the observations. The normalization is shown in Figure 7, along with the experimental observations.

One of the disturbing factors in the preceding development is that it was necessary to postulate that the temperature and area were higher than those initially assumed. Also, the calculated integrated density does not fall off as rapidly, at long times, as that observed. This latter is of course a result of the neglect of the effect of thermal conduction into the interior.

Let us consider an alternate approach to the problem. Suppose we assume that a finite thickness of material is heated to the initial temperature T_o and that the thermal conductivity of this very hot layer is sufficient so that a constant temperature is maintained throughout the layer, then the rate of cooling (neglecting thermal conductivity into the interior) is given by

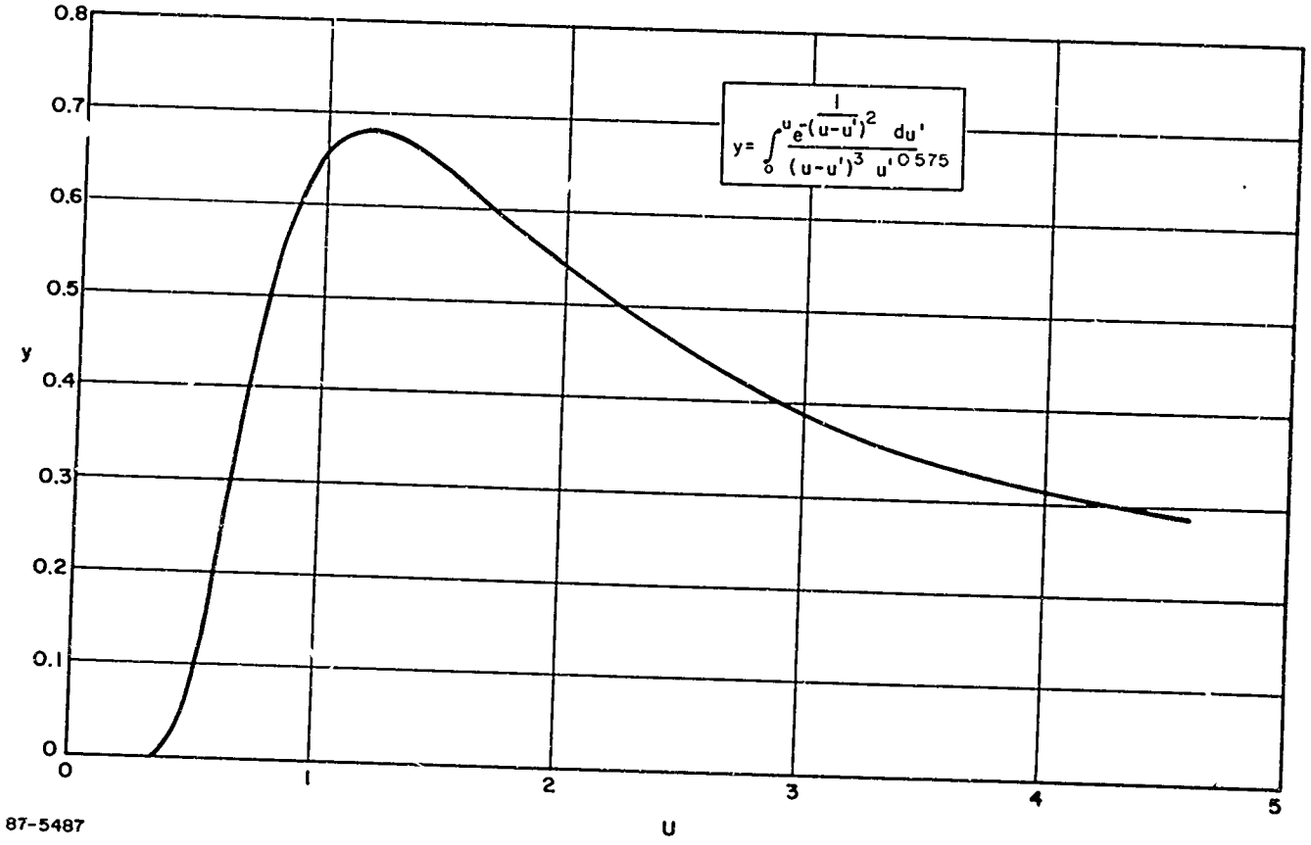

Figure 6 INTEGRATION OF EQUATION (32)

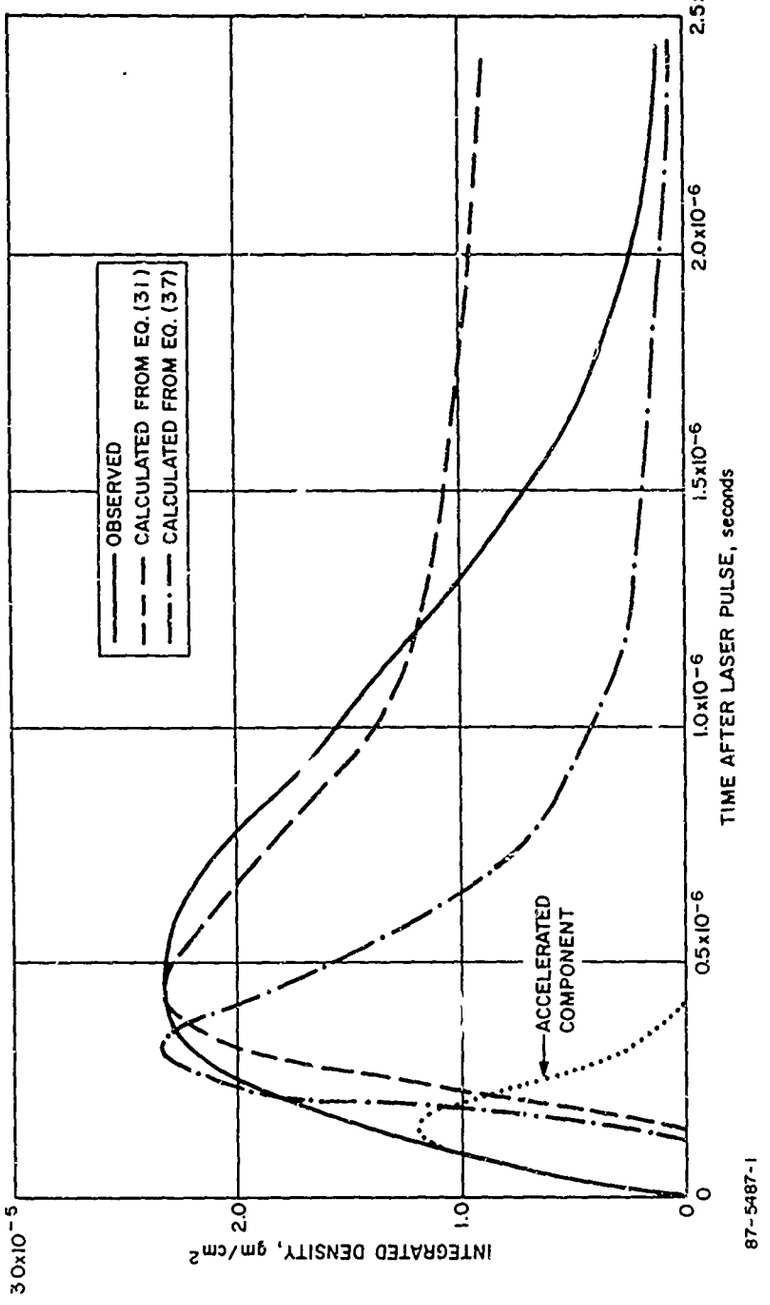

Figure 7 INTEGRATED DENSITY VERSUS TIME

$$\frac{dT}{dt} = - \frac{8 \times 10^{13} \, (exp^{-1.03 \times 10^5 / T})}{\rho C \delta}$$

$$\int_T^{T_o} exp \; 1.03 \times 10^5/T \; dT = \frac{8 \times 10^{13} \, t}{\rho C \delta} \tag{33}$$

The expression on the left has already been evaluated, and the resulting expressions for mass evaporation rate and temperature are, using ρC = 5 joule/cm^3,

$$\dot{m} = \frac{1.02 \times 10^{-2}}{(t/\delta + 2.38 \times 10^{-10} exp \; 8.95 \times 10^4 / T_o)^{1.15}} \tag{34}$$

$$T = 8.95 \times 10^4 \; [ln \; (4.9 \times 10^9 \; t/\delta + exp \; 8.9 \times 10^4 / T_o)]^{-i} \tag{35}$$

Equation (35) indicates a slow variation in T for most of the elapsed time. Again, we can estimate an average temperature by choosing a constant temperature which gives the same emission. In one microsecond, Equation (34) gives an emission of 1.0 x 10^{-4} gm/cm^2, for an average temperature of 6320°K, for a δ of 3 x 10^{-4} cm, and T_o = 10^4°K. We must then evaluate the equation

$$\int_{-\infty}^{\infty} \rho \, dx = \frac{2}{\sqrt{\pi}} (1.02 \times 10^{-2}) \pi a^2 \left(\frac{M}{2R\bar{T}}\right) Z \int_{t'=0}^{t} \frac{e^{-\frac{M z^2}{2R\bar{T}(t-t')^2}}}{(t-t')^3 \, (t/\delta + 2.38 \times 10^{-10} \, exp \, 8.98 \times 10^9/T_o)^{1.15}} \, dt' \tag{36}$$

Again, this equation must be numerically integrated. If we let

$$u = \sqrt{\frac{2RT}{M}} \cdot \frac{t}{z}$$

we have

$$\int_{-\infty}^{\infty} \rho \, dx = \frac{2A}{\sqrt{\pi}} (1.02 \times 10^{-2}) \left(\frac{M}{2RT}\right)^{-0.075} z^{-2.15} \, \delta^{1.15} \int_0^u \frac{e^{-\frac{1}{(u-u')^2}}}{(u-u')^3 \, (b+u')^{1.15}} \, du' \tag{37}$$

When

$$b = \frac{2.38 \times 10^{-10} \delta \exp 8.95 \times 10^4 / T_o}{\sqrt{M z^2 / 2RT}}$$

for $T_o = 10^4$, $Z = 0.1$, $T = 6.1 \times 10^3$, and $\delta = 3 \times 10^{-4}$ cm,

$$u = 2.97 \times 10^6 \; t,$$

$$b = 1.6 \times 10^{-3},$$

and

$$\int_{-\infty}^{\infty} \rho \, dx = 9.52 \times 10^{-4} \; A \int_0^u \frac{e^{-\frac{1}{\omega^2}} \, d\omega}{\omega^3 \, (-\omega + 1.6 \times 10^{-3} + u)^{1.15}} \qquad (38)$$

Figure 8 gives the results of the numerical evaluation. The integral has a maximum value of 3.85 occurring at $u = 0.92$. This corresponds to an integrated density (using $A = 2 \times 10^{-3}$) of 7.3×10^{-6} at a time of 3.1×10^{-7} seconds. The integrated density is about a factor of 6 too low, however it is again reasonable to assume that the area evaporating is larger than the irradiated area.

Figure 7 shows the results of these two approaches, as well as the observed result. Both calculated curves are normalized to give the same peak integrated density.

The curve for the infinite slab case appears to provide a better approximation at times near the peak of the integrated density, whereas the curve for the finite slab appears best for much longer times. At short times, the two curves are approximately equal (after normalization), and neither accounts for the observed density. The dashed line shows the difference between the calculated and observed values at short times. This difference is assumed to be the high-velocity component of the vapor emitted by the target, i.e., the vapor which has been accelerated by gaining energy from the laser beam.

D. OBSERVATIONS AT LARGER DISTANCES

The data presented in Figure 3 (and repeated in Figure 7) are typical of all the data taken at short distances from the target. To be sure, there are variations, but not of a significant nature. Figure 9 presents some data obtained at a longer distance (3mm from target). Again, this does not differ greatly from that obtained at the shorter distance. There is, however, a tendency towards a separation of the high- and low-velocity components. This tendency is presumably fortuitous, since it is not always observed. It can be accounted for, if the relative amount of the higher velocity component is increased over the one given

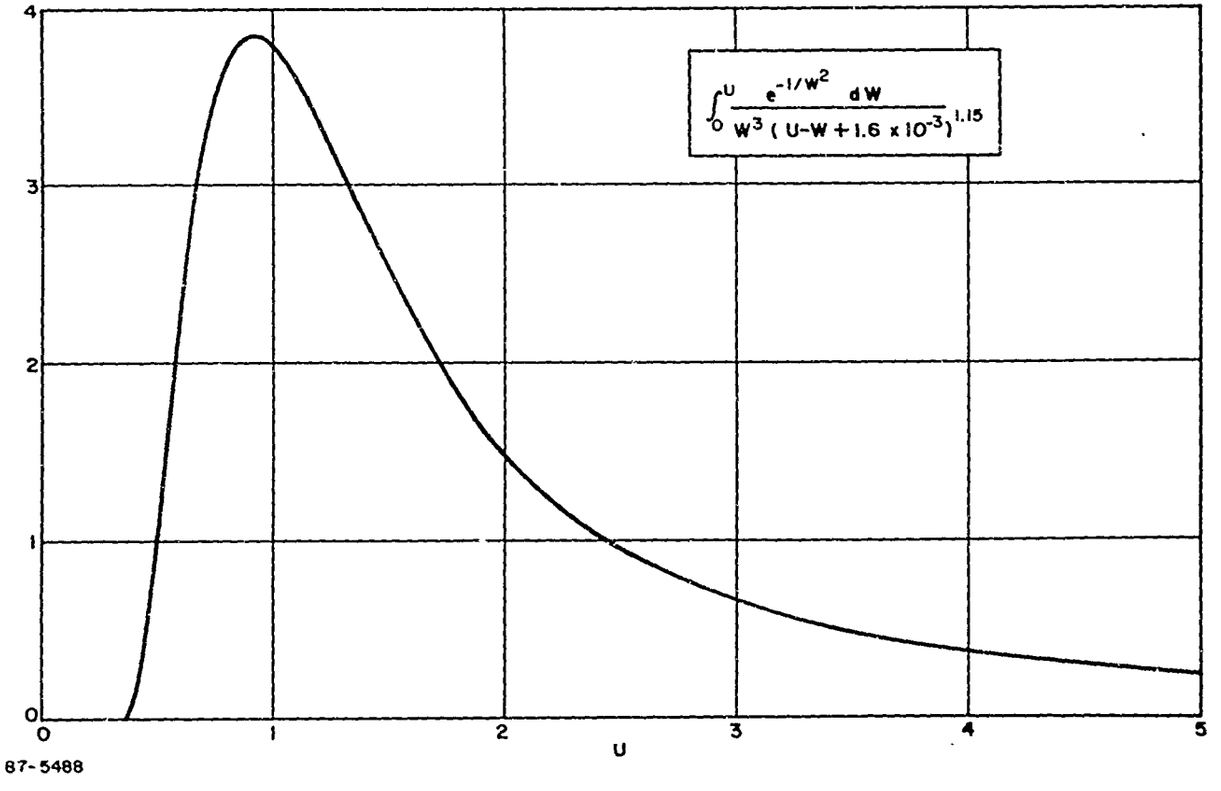

Figure 8 INTEGRATION OF EQUATION (38)

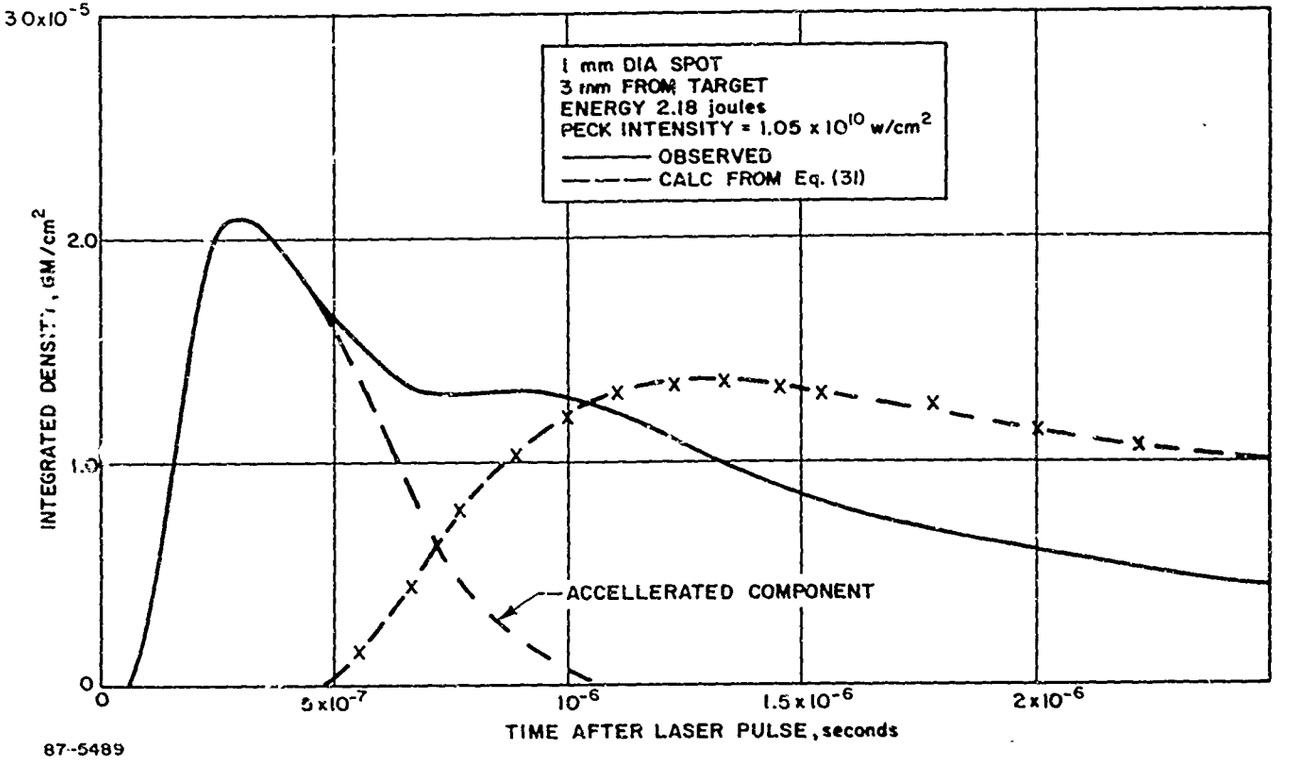

Figure 9 INTEGRATED DENSITY VERSUS TIME

in Figure 3. In Figure 9, Equation (32) was fitted, approximately, to the value of integrated density at 10^{-6} seconds. The agreement is only qualitative, since the time of the maximum appears to be too long. The accelerated component was obtained by subtracting the calculated value from the observations. The maximum of this component occurs at a time which is approximately three times longer than the maximum of Figure 3 -- as is to be expected.

E. UNFOLDING

The original concept of the experiment included the unfolding of the integrated density to obtain an instantaneous spatially resolved mass density. However, the data were found to contain too much scatter to permit such an unfolding. In order to unfold the data, it would be necessary to perform many more observations to get reasonably good averages of the integrated density at a given condition.

As will be discussed later, this effort does not appear to be warranted, especially since the mass density experiment does not provide data which can readily be interpreted in terms of the high intensity effects toward which the experiment was directed.

IV. CONCLUSION

The use of the electron beam technique to determine the mass density of the laser blowoff has turned out to be of doubtful value, not because the experiment was unsuccessful, but because the technique responded to effects which were not properly a part of the high intensity interaction.

It was originally hoped that the mass density approach would confirm the details of theoretical models on the interaction. However, the experimental results themselves indicate that the bulk of the experimental results are due, not to plasma created during the time duration of the laser pulse, but to the vapor which has been thermally emitted from the hot target after the pulse.

This result is in itself of interest, since it can account for phenomena which have been observed in other experiments. One such phenomena is the observation of radiative decay of species driven from a solid target by laser radiation.* The observations tend to give lifetimes longer than could reasonably be obtained if the vapor left the vicinity of the target in a time which was characteristic of thermal evaporation during the laser pulse alone.

In order to use the electron beam technique to probe events that occur close to the surface, it is necessary to concentrate on the first event during the laser pulse. In the experiments that have been performed, the whole event was observed, so that the oscilloscope traces of the electron beam current were observed for times of typically 2 to 4 microseconds; consequently, when the effort to observe the whole event was made, the time resolution necessary to perform an analyses for the first few tens of nanoseconds was lost.

We have now found, however, that the whole event is not meaningful for the high-intensity interaction. In fact, the only part of the high-intensity interaction which can be observed with the electron beam technique is the part that occurs before the leading edge of the low-velocity vapor, thermally emitted from the target, has reached the position of the electron beam.

* Private communication from T. Wentink, Avco/SSD.

APPENDIXES

A. EVAPORATION PROPERTIES OF GRAPHITE

B. DERIVATION OF DENSITY EQUATIONS

APPENDIX A

EVAPORATIVE PROPERTIES OF GRAPHITE

The vapor pressure of graphite is published as a function of temperature e.* If the vapor pressure is known, the mass evaporation rate can be determined from kinetic theory to be

$$\dot{m} = p/(2\pi RT)^{1/2} \tag{A1}$$

where p is the pressure in dyne/cm^2, and R is the gas constant per gram.

From the published data, we then obtain:

p = 1 torr	T = 3859° K	$\dot{m}$ = 3.26 x 10^{-3}
10	4219	3.12 x 10^{-2}
40	4469	1.21 x 10^{-1}
100	4646	2.97 x 10^{-1}
400	4933	1.15 x 10^{0}
760	5100	2.14 x 10^{0}

This can be fitted quite accurately with the equation

$$\dot{m} = 1.2 \times 10^{9} \exp(-1.03 \times 10^{5}/T)\ gm/cm^2\text{-}sec \tag{A2}$$

The latent heat of evaporation of graphite is 172 kcal/mole, 6.0 x 10^4 joule/gm. Since the energy required to evaporate 1 gm of graphite at a temperature T is $E = 6 \times 10^4 + 2RT/M$, the power per unit area involved in evaporation is

$$I = (6 \times 10^{4} + 1.39\,T)\,\dot{m} \quad watt/cm^2 \tag{A3}$$

This can be approximated by

$$I = 8.0 \times 10^{13} \exp(-1.03 \times 10^{5}/T)\ watt/cm^2 \tag{A4}$$

* Handbook of Chemistry and Physics, 41st Edition.

APPENDIX B

DERIVATION OF DENSITY EQUATIONS

Let us estimate the density to be expected from the vapor evaporated by a hot surface. To perform the calculations, we will assume that the vapor is Maxwellian, with a temperature T characteristic of the surface. From kinetic theory, the velocity distribution function of a gas evaporating from a surface at a temperature T is

$$N(v)\,dv\,d\Omega = (2/\pi)\,(M/2RT)^2\,v^3\cos\theta\,(\exp - Mv^2/2RT)\,dv\,d\Omega \tag{B1}$$

and is the fraction emitted in the direction θ, measured from the normal, in the solid angle $d\Omega$ and in the velocity range from v to $v + dv$. If the total mass evaporation rate per unit area is $\dot{m}$, then the mass evaporation rate per unit surface area, in the same velocity range, direction, and solid angle, is

$$\dot{m}\,N(v)\,dv\,d\Omega$$

We can determine the density at a distance r from the point of evaporation, due to the mass emitted in a time dt', by first determining the mass evaporated and dividing this by the volume occupied by the vapor. The evaporated mass in the velocity range v to $v + dv$, direction θ, solid angle $d\Omega$, and timed dt', per unit surface area is,

$$dm = \dot{m}\,N(v)\,dv\,d\Omega\,dt' \tag{B2}$$

The volume occupied by this vapor is a shell of area $r^2\,d\Omega$ and thickness $v\,dt'$ Thus the density is

$$d\rho = \dot{m}\,(2/\pi)\,(M/2RT)\,[v^2\cos\theta/r^2\exp(-Mv^2/2RT)]\,dv \tag{B3}$$

At a time t, the velocity v corresponding to evaporation at a time t s

$$v = r/(t-t') \tag{B4}$$

where t' is the time of evaporation and t is the time of observation.

Thus

$$dv = r\,dt'/(t-t')^2 \tag{B5}$$

Also, $\cos\theta = z/r$, where z is the distance normal to the surface. We then have

$$d\rho = \dot{m}\,(2/\pi)\,(M/2RT)^2\,(t-t')^{-4}\,z\,\{\exp[-Mr^2/2RT(t-t')^2]\}\,dt' \tag{B6}$$

The experimental observations, however, are of the integrated density along a line parallel with the surface. Equation (B6) can be integrated along a line parallel to the surface. Letting $r^2 = x^2 + y^2 + z^2$, we have

$$d\int_{-\infty}^{\infty}\rho\,dx = \dot{m}\,z\,(2/\pi)\,(M/2RT)^2\,(t-t')^{-4}\,\exp\left[\frac{-M(y^2+z^2)}{2RT\,(t-t')^2}\right]dt'\,2\int_0^{\infty}\exp\left[\frac{-Mx^2}{2RT(t-t')^2}\right]dx$$

$$d\int_{-\infty}^{\infty}\rho\,dx = \dot{m}\,z(2/\sqrt{\pi})\left(\frac{M}{2RT}\right)^{3/2}(t-t')^{-3}\,\exp\left[\frac{-M(y^2+z^2)}{2RT(t-t')^2}\right]dt' \tag{B7}$$

This expression can be integrated over t' , if desired. However, we have not considered the effect of the finite source area. If we consider a circular source area, we have, for the density integrated along a line passing through the normal to the center of the source,

$$\int_{-\infty}^{\infty}\rho\,dx = \frac{8}{\sqrt{\pi}}\,\dot{m}\,L\left(\frac{M}{2RT}\right)^{3/2}(t-t')^{-3}\exp\left[-\frac{Mz^2}{2RT(t-t')^2}\right]\left(\int_0^a\sqrt{a^2-y^2}\,\exp\left[-\frac{My^2}{2RT(t-t')^2}\right]dy\right)dt' \tag{B8}$$

The integral is equivalent to the integral

$$a^2\int_0^1\sqrt{1-u^2}\;\;e^{-bu^2}\,du \tag{B9}$$

where

$$b = \frac{M a^2}{2RT(t-t')^2} \tag{B10}$$

This integral can be evaluated with the series

$$\frac{a^2 \pi}{4} \left[1 - \frac{b}{4} + \frac{b^2}{16} - \frac{5b^3}{384} + \frac{7b^4}{3072} + \cdots + \frac{(-1)^n [1 \cdot 3 \cdot 5 \cdots (2n-1)]}{(n+1)!\ n!\ 2^n} b^n \right] \tag{B11}$$

When b is large, it becomes

$$\frac{\sqrt{\pi}}{2\sqrt{b}} \tag{B12}$$

The value of this integral is plotted as a function of b in Figure B1.

In the practical case, however, z is usually larger than a. Also, the overall expression has a negligible value when

$$\frac{M z^2}{2RT(t-t')^2}$$

is greater than about 4. Thus, it appears legitimate to neglect the effect of the finite area, for $z > a$, and use

$$d \int_{-\infty}^{\infty} \rho\, dx = 2\sqrt{\pi}\, a^2 \dot{M} z \left(\frac{M}{2RT}\right)^{3/2} (t-t')^{-3} \exp\left[- \frac{M z^2}{2RT(t-t')^2} \right] dt' \tag{B13}$$

which can be integrated to give

$$\int_{-\infty}^{\infty} \rho\, dx = \sqrt{\pi}\, \dot{m}\, a^2 \left(\frac{M}{2RT}\right)^{1/2} z^{-1} \left[\exp\left(\frac{-M z^2}{2RT\, t^2}\right) - \exp \frac{-M z^2}{2RT(t-t')^2} \right] \tag{B14}$$

if $\dot{m}$ is constant from $t = 0$ to t'.

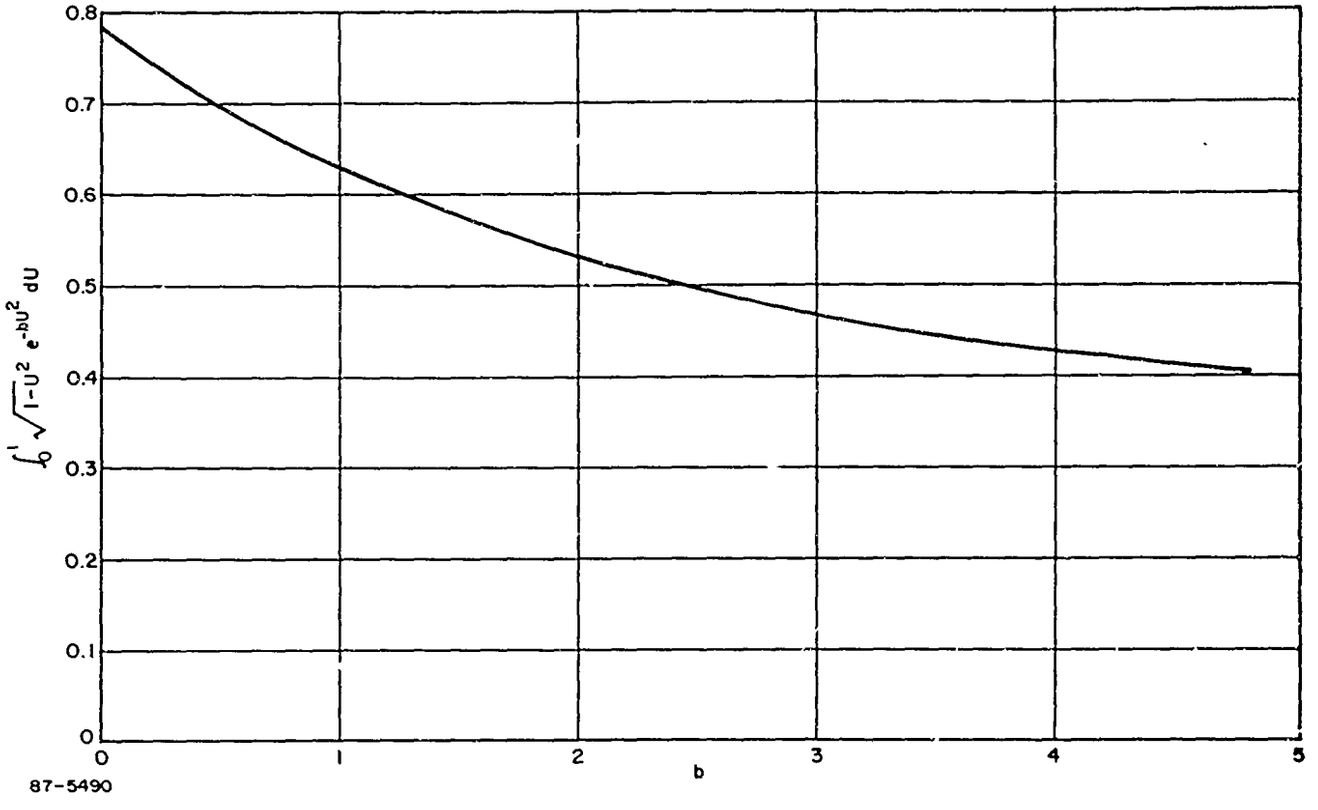

F'gure B1 INTEGRATION OF EQUATION (B9)

Even if z is less than a, it can be seen from Figure B1 that the integral over the surface area is not a very rapidly varying function. It therefore appears reasonable to use the value of the integral of the point at which

$$d \int_{-\infty}^{\infty} \rho \, dx$$

is a maximum. The maximum of Equation (B8) occurs approximately when

$$1.5\,(t-t') = \frac{M z^2}{2RT} \tag{B15}$$

or when

$$b = \frac{M a^2}{2RT(t-t')^2} = 1.5\, a^2 z^2 \tag{B16}$$

When b is less than 5, the graph of Figure B1 is applicable. When b is larger, the integral can be approximated quite well by

$$\frac{\sqrt{\pi}}{2\sqrt{b}} = \frac{0.72\, z}{a} \tag{B17}$$

Thus

$$d \int_{-\infty}^{\infty} \rho \, dx = 3.28\, \dot{m}\, a\, z^2 \left(\frac{M}{2RT}\right)^{3/2} (t-t')^{-3} \exp\left[-\frac{M z^2}{2RT(t-t')^2}\right] dt' \tag{B18}$$

when $a > 2z$, and

$$d \int_{-\infty}^{\infty} \rho \, dx = 3.54\, \dot{m}\, a^2 z \left(\frac{M}{2RT}\right)^{3/2} (t-t')^{-3} \exp\left[-\frac{M z^2}{2RT(t-t')^2}\right] dt' \tag{B19}$$

when $a < z$.

For $\dot{m}$ = constant from $t' = 0$ to $t' = t'$, we then have

$$\int_{-\infty}^{\infty} \rho \, dx = 1.64 \, \dot{m} \, a^2 \left(\frac{M}{2RT}\right)^{1/2} \left[exp - \frac{M z^2}{2RT(t)^2} - exp - \frac{M z^2}{2RT(t-t')^2}\right] \tag{B20}$$

for $a > 2z$, and

$$\int_{-\infty}^{\infty} \rho \, dx = \frac{1.77 \, \dot{m} \, a}{z} \left(\frac{M}{2RT}\right)^{1/2} \left[exp - \frac{M z^2}{2RT t^2} - exp - \frac{M z^2}{2RT(t-t')^2}\right] \tag{B21}$$

if $a < z$.

Unclassified
Security Classification

DOCUMENT CONTROL DATA - R & D

(Security classification of title, body of abstract and indexing annotation must be entered when the overall report is classified)

1. ORIGINATING ACTIVITY (Corporate author) AVCO Missiles, Space & Electronics Group Space Systems Division 201 Lowell Street, Wilmington, Massachusetts	2a. REPORT SECURITY CLASSIFICATION Unclassified 2b. GROUP

3. REPORT TITLE

LASER INDUCED SURFACE EFFECTS

4. DESCRIPTIVE NOTES (Type of report and inclusive dates)

Final Technical Report

5. AUTHOR(S) (First name, middle initial, last name)

R. Schlier and J. Shumsky

6. REPORT DATE	7a. TOTAL NO. OF PAGES	7b. NO. OF REFS
10 July 1967	40	

8a. CONTRACT OR GRANT NO.	9a. ORIGINATOR'S REPORT NUMBER(S)
DA-19-020-AMC-00521(X) b. PROJECT NO.	AVSSD-0244-67-RR
c. d.	9b. OTHER REPORT NO(S) (Any other numbers that may be assigned this report)

10. DISTRIBUTION STATEMENT

Distribution of this document is unlimited.

11. SUPPLEMENTARY NOTES	12. SPONSORING MILITARY ACTIVITY
	U.S. Army Ballistic Research Laboratories Aberdeen Proving Ground, Maryland

13. ABSTRACT

This document presents the results of experiments in which a moderate energy electron beam was used to probe the plasma created by a laser beam impinging on a graphite target.

DD FORM 1 NOV 65 1473 REPLACES DD FORM 1473, 1 JAN 64, WHICH IS OBSOLETE FOR ARMY USE.

Unclassified
Security Classification

Unclassified
Security Classification

KEY WORDS	LINK A		LINK B		LINK C	
	ROLE	WT	ROLE	WT	ROLE	WT
Electron Beam						
Probe						
Plasma						
Laser						

Unclassified
Security Classification